Banafsheh Barabadi

Yogendra K. Joshi[1]

Satish Kumar

G.W. Woodruff School of Mechanical Engineering, Georgia Institute of Technology, Atlanta, GA, 30332

Gamal Refai-Ahmed

Advanced Micro Devices, Inc., Markham, ON, Canada, L3T-7X6

Interconnect Joule Heating under Transient Currents using the Transmission Line Matrix Method

The quality and reliability of interconnects in microelectronics is a major challenge considering the increasing level of integration and high current densities. This work studied the problem of transient Joule heating in interconnects in a two-dimensional (2D) inhomogeneous domain using the transmission line matrix (TLM) method. Computational efficiency of the TLM method and its ability to accept non-uniform 2D and 3D mesh and variable time step makes it a good candidate for multi-scale analysis of Joule heating in on-chip interconnects. The TLM method was implemented with link-resistor (LR) and link-line (LL) formulations, and the results were compared with a finite element (FE) model. The overall behavior of the TLM models were in good agreement with the FE model while, near the heat source, the transient TLM solutions developed slower than the FE solution. The steady-state results of the TLM and FE models were identical. The two TLM formulations yielded slightly different transient results, with the LL result growing slower, particularly at the source boundary and becoming unstable at short time-steps. It was concluded that the LR formulation is more accurate for transient thermal analysis. [DOI: 10.1115/1.4006137]

Keywords: Joule heating, transient, thermal modeling

Introduction

A major concern in the design of microprocessors is the quality and reliability of on-chip interconnects [1]. These interconnects are usually Al-Cu- or Cu-based submicron lines deposited on an insulation layer. Because of the increasing level of integration in microprocessors, interconnects are subjected to high current density and; hence, to high temperature increase under operating conditions. Moreover, because of the large thermal expansion mismatch between the metallic line and the underlying dielectric layer, high thermomechanical stresses develop. Several experimental and computational studies suggest that these factors are primarily responsible for morphological changes in the lines that result in open-circuit and short-circuit failures in interconnects and as a consequence, limiting the quality and reliability of the entire circuit. As an example, the basic elements of thermomechanical fatigue behavior of microelectronic interconnect structures, such as lines and vias, based on accelerated test results have been studied and FE analysis has been developed [2].

Interconnect lines always contain a variety of pre-existing defects such as voids and cracks [3]. Local hot spots, which originate from these defects, often have a major role in controlling the micro-mechanisms of interconnect line failures. Such failure processes are governed by the kinetics of inhomogeneous diffusions and/or reactions. For example, the effect of electromigration, as well as the variation of diffusion rates, will accelerate void growth and translation, and their accompanied stress buildups, leading to a final failure of the interconnect line. The transient heat transfer in the system greatly influences the morphology of failure and the pattern of damage evolution, which depend strongly on the electric current loading rate.

The problem of steady state Joule heating in interconnects has been studied using 2D analytical, finite difference (FD), and finite element (FE) 2D and 3D models [4–6]. Multi-stack interconnect architecture is characterized by wide range of length scales (from 10^{-9} m to 10^{-2} m) and significant material inhomogeneity (thermal conductivity variation from 0.1 W/mK to 400 W/mK). Different metal levels are connected through vias that provide electrical connections. To reduce the total simulation time, it is often desirable to use an inhomogeneous mesh that is more refined in the areas if there is large temperature gradient. In existing FD and FE models, computational times are long even for a unit cell (micro-models). Some authors have proposed compact FE models to reduce the computational time, with the trade-off being reduced resolution and accuracy especially at the interface between the metal and dielectric [7,8]. It has been shown that using the method of quad-tree mesh with the TLM method as well as algorithms for optimizing the time stepping can reduces the execution time by 100 times [9].

Recent multicore chip architectures which incorporate dynamic migration of computing loads point to the importance of Joule heating under transient conditions. In the present study, we investigate transient heating effects using the Transmission Line Matrix (TLM) Method [10,11]. The TLM formulation is based on a resistance and capacitance network and allows for temperature-dependent and inhomogeneous material parameters, non-uniform mesh, and variable time-stepping. The conventional link-line (LL) TLM network used for 1D diffusion problems often results in numerical oscillations [12]. The link resistor (LR) method, with capacitance centered on the nodes, with resistors placed mid-way between nodes, contrasts with the LL method, in which resistors are placed at the nodes, with transmission lines linking adjacent nodes, yielding reduced oscillations. Comparisons between various LL and LR models indicate that, in general, 2D LR TLM models consistently produce more accurate results [12]. It should be noted that, once the domain is approximated by a TLM model, the TLM solution is exact. The approximation of a TLM model is in the analogy of the physical system (in this case, heat diffusion) with an electrical circuit. In contrast, two approximations exist in

[1]Corresponding author. Yogendra K. Joshi, Ph.D., G.W. Woodruff School of Mechanical Engineering, Georgia Institute of Technology, 801 Ferst Dr, Atlanta, GA, 30332.

Contributed by the Electronic and Photonic Packaging Division of ASME for publication in the Journal of Electronic Packaging. Manuscript received July 19, 2010; final manuscript received December 2, 2011; published online March 21, 2012. Assoc. Editor: Koneru Ramakrishna.

 Copyright © 2012 by ASME

Downloaded From: http://electronicpackaging.asmedigitalcollection.asme.org/ on 01/08/2014 Terms of Use: http://asme.org/terms

the FE model: one approximation is in dividing the given geometry into elements, the other is in approximating the solution in an element. It is important to note that nonlinear material properties, dependent on time or temperature, can be implemented in the TLM algorithm as described by several authors in the literature (e.g., Refs. [10] and [11]).

Another advantage of the TLM method over FD and FE methods is greater stability. In particular, for transient thermal analysis, this allows the time step to be increased as the simulation progresses towards steady state; hence reducing the computational time significantly. Moreover, TLM has the possible use in multiscale simulations by incorporating rapid local zoom-in approaches such as the quad-tree mesh [9–11].

TLM Background

The original TLM differential equation is a hyperbolic equation, which indicates that this method can also be used to simulate the hyperbolic heat equation that is based on the Cattaneo equation. The Cattaneo equation has been proposed as a more general form of Fourier's law and many researchers believe that Cattaneo's equation extends the validation regime of Fourier's law to time scales shorter than the relaxation time of a material. Cattaneo's equation leads to a form of heat equation known as the hyperbolic heat equation, which is a damped wave equation that predicts heat will propagate in waves with a finite speed. However, because of the lack of convincing experimental evidence and contradictions with the second law of thermodynamics, justification for accepting Cattaneo's equation has been questioned [13]. Several phenomenological theories have been developed to describe transient heat transfer processes in solids and micro-/nano-structures. Applications of transient and ultra-fast heating include laser processing, nanothermal fabrication, and the measurement of thermophysical properties. In the literature, there appears to be controversial experimental evidence on the existence of certain phenomena predicted by the hyperbolic heat conduction. Furthermore, there exists a large division regarding the formulation and the interpretation of the theories of non-Fourier conduction. Consequently, to avoid the issues associated with hyperbolic heat conduction equation, the propagation term in Eq. (1) is kept small and negligible (see below), such that the analogous heat equation (Eq. (5)) can be approximated. As described in the following section, this is verified with keeping the parameter m much smaller than unity.

Formulation

An electrical impulse in a transmission line matrix can be formulated using the Maxwell's curl equation for propagation in a lossy medium, also known as the Telegrapher's Equation [14]:

$$\nabla^2 V = L_d C_d \frac{\partial^2 V}{\partial t^2} + R_d C_d \frac{\partial V}{\partial t} - \frac{R_d}{\Delta x} I \quad (1)$$

where, L_d, C_d, and R_d are the distributed electrical inductance, capacitance, and resistance per unit length in the transmission line, respectively. V and I are the nodal voltage and current in the electrical circuit.

Eq. (1) and transient heat conduction equation (Eq. (5)) have a similar structure. In Eq. (1), voltage can be treated as temperature ($V \equiv T$) and a network of electrical circuit elements can simulate the medium, which means that temperature propagates in the form of a damped wave. This is only valid on the grounds that the space and time discretizations are properly chosen (explained in this section). Using this approach, the transient heat conduction equation can be solved explicitly. Some advantages of this method can be found in Refs. [10,11]. Analytical solution of the transient heat conduction equation for interconnects is complicated due to: (a) non-continuum transport effects at sub 40 nm for copper, (b) transient heat transfer at short-time scales associated with device operational frequencies, (c) the large variation in thermal properties of the material from metals to dielectrics, and (d) the non-uniformity of heat generation at the base of devices [13]. TLM based formulation is of great value in simulations involving micro/nano-length and -time scales, variation in thermal properties and non-uniform power generation. The physical interpretation of the coefficients of Eq. (1) is related to the thermal parameters as described in the following analogies:

$$R_d C_d \equiv \frac{1}{\alpha} = \frac{\rho C_P}{\kappa} \quad (2)$$

where α is the diffusion coefficient, and

$$L_d C_d \equiv \frac{1}{v_{\mathrm{tw}}^2} \quad (3)$$

where v_{tw} is the speed of the temperature wave. By dividing Eq. (3) by Eq. (2), it can be seen that the relaxation time of the temperature wave, which is interpreted as the time of the collision of the particles [13], can be written as

$$\tau \equiv \frac{L_d C_d}{R_d C_d} = \frac{L_d}{R_d} \quad (4)$$

By substituting the thermal equivalence of the parameters back into the Eq. (1), the Telegrapher's Equation can be reduced to the transient heat conduction equation:

$$\nabla(\kappa(T)\nabla T) = \rho C_P \frac{\partial T}{\partial t} - g(x, y, z, t) \quad (5)$$

where $\kappa(T)$ is the thermal conductivity as a function of temperature, C_p is the specific heat of the material, ρ is the material density, and $g(x,y,z,t)$ represents the local instantaneous volumetric heat generation.

Notably, the first term on the right-hand side of Eq. (1), the propagation term, has no equivalent in the classical heat diffusion equation (Eq. (5)), and is therefore an error term in transmission line modeling of diffusion problems. The error term is negligible when [15]

$$R_d C_d \frac{\partial V}{\partial t} >> L_d C_d \frac{\partial^2 V}{\partial t^2} \quad (6)$$

By defining the parameter m as

$$m = L_d C_d \frac{\partial^2 V}{\partial t^2} \bigg/ R_d C_d \frac{\partial V}{\partial t} \quad (7)$$

The restriction in Eq. (6) can be restated as $m \ll 1$. The error parameter m, for a 2D heat diffusion problem with diffusion coefficient α, can be written as [15]

$$m = \alpha \frac{\Delta t^2}{\Delta x^2} \left[\frac{\partial^2 V}{\partial t^2} \bigg/ \frac{\partial V}{\partial t} \right] \quad (8)$$

which shows that m is a function of both time step and spatial resolution. The parameter m is a measure of how accurately the Telegrapher's equation (Eq. (1)) models the diffusion equation. It is not a measure of the accuracy of the numerical solution to the particular problem, which ultimately depends on the spatial resolution and time step, Δx and Δt. The parameter m allows determination of an appropriate choice of Δt for the Δx being employed.

Once R_d and C_d have been determined by the physical problem, a requirement that the pulses travel from node to node in a time

Downloaded From: http://electronicpackaging.asmedigitalcollection.asme.org/ on 01/08/2014 Terms of Use: http://asme.org/terms

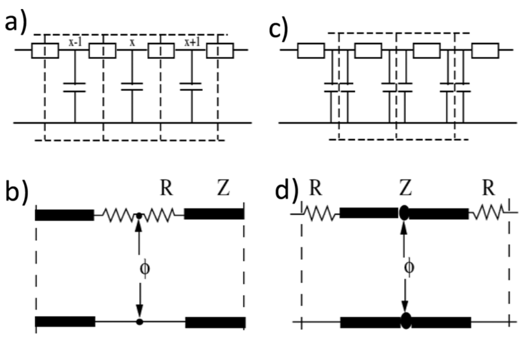

Fig. 1 Analogous electrical circuit for (*a*) link-line TLM (LL TLM) method and (*c*) link-resistor TLM (LR TLM) method. Electrical circuit representation of a single node of resistance-impedance network by (*b*) LL TLM and (*d*) LR TLM methods [11].

step Δt results in the complex transmission line impedance Z being equal to $\Delta t/(C_d \Delta x)$, where Δx is the local distance between nodes. The requirement that the second term in Eq. (1) be negligible then becomes a condition that Δt must be sufficiently small [9].

Methodology

The TLM approach is described here primarily following [10,11]. The TLM method is built on the rules governing the travel of potential pulses. In a 1D horizontal model (Fig. 1), the incident pulse at an arbitrary node (x) travels along the transmission lines approaching the node from either left or right. This pulse will then be scattered passing the node. It either gets reflected back in the same line with the reflection coefficient ρ, or gets transmitted with the transmission coefficient τ. These coefficients are calculated based on the encountered resistance and impedance on the transmission line. A voltage impulse entering a LL node will travel along a transmission line during a time $\Delta t/2$. At this point, it encounters a discontinuity, $Z_T = (R + R + Z)$. The reflection coefficient $\rho = (Z_T - Z)/(Z_T + Z)$ is then

$$\rho = \frac{R}{R+Z} \tag{9}$$

Based on the fact that $\rho + \tau = 1$, the transmission coefficient will be

$$\tau = \frac{Z}{R+Z} \tag{10}$$

The equivalent discretizations of the medium are analogous electrical network methods shown in Figs. 1(*a*) and 1(*c*). If the impedances are located at the interface between the nodes, it is called a Link-line (LL) representation (Fig. 1(*b*)). On the other hand, if the resistors are placed at the interface, it is called a Link-Resistor (LR) representation, which is implemented in the present work and shown in Fig. 1(*d*). To write the equation of transmission line based on the electrical equivalent circuit, we focus on the three adjacent nodes in the line (x), $(x+1)$, and $(x-1)$ demonstrated in Fig. 2. At the start of an iteration, six pulses share these three positions, which are situated at the center of transmission lines. The interaction of these waves is described below and in Fig. 2.

The incident pulses from left and right for node (x) at any time step are a combination of the pulses that have been scattered at the previous time step from the adjacent nodes and node (x) itself. In other words, the pulse that is at $(x-1)$ traveling to the left is no longer relevant to node (x) and is ignored. The same applies to the one that is traveling to the right from $(x+1)$. These two pulses are shown with dotted line arrows. The other four pulses travel for time $\Delta t/2$ before they are scattered at the resistors. They are shown as dashed line arrows. They then become incident on (x) from left and right, shown with solid line arrows. The formulation will then be in the forms of:

(a) Incident pulse for node (x) at time step $k+1$:

$$\begin{aligned} {}_{k+1}{}^{i}V_L(x) &= \rho\,{}_k^{s}V_L(x) + \tau\,{}_k^{s}V_R(x-1) \\ {}_{k+1}{}^{i}V_R(x) &= \rho\,{}_k^{s}V_R(x) + \tau\,{}_k^{s}V_L(x+1) \end{aligned} \tag{11}$$

(b) Scattered pulse for node (x) at time step $k+1$. When an incident pulse passes a node from one side to another, it switches from incident to scattered:

$$\begin{aligned} {}_{k+1}^{s}V_L(x) &= {}_{k+1}^{i}V_R(x) \\ {}_{k+1}^{s}V_R(x) &= {}_{k+1}^{i}V_L(x) \end{aligned} \tag{12}$$

(c) Instantaneous potential at node (x) at time step $k+1$ is written as the summation of simultaneously arriving pulses at the node:

$$ {}_{k+1}V = {}_{k+1}^{i}V_L(x) + {}_{k+1}^{i}V_R(x) \tag{13}$$

To complete the algorithm, Eqs. (11) – (13) are repeated for k iterations, where $k\Delta t$ is the total time of simulation.

Two types of boundary conditions (BCs) were considered in this work. As a heat pulse reaches an insulating boundary, it gets reflected back into the physical domain. This is equivalent to an open-circuit $(\rho = 1)$ condition. This condition should be applied at the interface between nodes. Hence, a pulse traveling from a node during time $\Delta t/2$ faces the boundary and arrives back at the node at the end of the time step. Assuming there is an insulating boundary on the right-hand side of the 1D model, using Eq. (11), this BC can be formulated as:

$$ {}_{k+1}^{i}V_L(x) = \rho\,{}_k^{s}V_L(x) + \tau\,{}_k^{s}V_R(x-1) \tag{14}$$

$$ {}_{k+1}^{i}V_R(x) = 1\,{}_k^{s}V_R(x) + 0\,{}_k^{s}V_L(x+1) \tag{15}$$

Eq. (15) can be simplified:

$$ {}_{k+1}{}^{i}V_R(x) = {}_k^{s}V_R(x) \tag{16}$$

For a constant temperature boundary, it is the resistor – not the transmission line – that touches the boundary. There are two

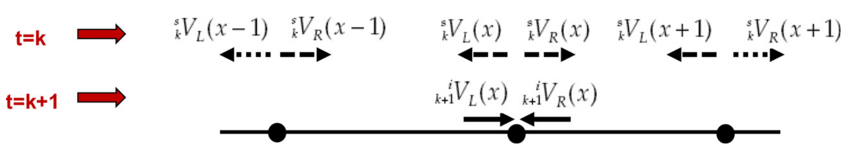

Fig. 2 Three adjacent nodes located at the center of transmission line and their pulses. Solid line arrows = incident pulse. Dashed and dotted line arrows = scattered pulse. Pulse notation for left superscript: s = scattered and i = incident. Pulse notation for left subscript: k = time step. Pulse notation for right subscript: pulse approaching the node from left (L) and from right (R).

Downloaded From: http://electronicpackaging.asmedigitalcollection.asme.org/ on 01/08/2014 Terms of Use: http://asme.org/terms

separate considerations in this BC: (a) the input from the source can now be placed at the boundary, and (b) the history of the pulse that is scattered from node 1 subsequently approaches the boundary. The source (V_C) on the boundary sees a series connection of resistor and impedance, so the standard potential divider formula gives the signal injected into the line. The pulse scattered toward the boundary sees a short circuit, so the total, which is incident from the left at a new time step, is the sum of these contributions. This can be formulated as

$$_{k+1}{}^{i}V_L(1) = V_C\left(\frac{Z}{R+Z}\right) + {}_k^s V_L(1)\left(\frac{R-Z}{R+Z}\right) \tag{17}$$

In the LL method, Eqs. (11), (12), and (13) are replaced by the following equations:

(a) At time k, two incident pulses travel along the transmission line and approach the center of the node (x) from left and right. We can write Eq. (13) for time k:

$$_kV = {}_k^i V_L(x) + {}_k^i V_R(x) \tag{18}$$

(b) Scattered pulse (reflection and transmission) for node (x) at time step k:

$$\begin{aligned} {}_k^s V_L(x) &= \rho_k^i V_L(x) + \tau_k^i V_R(x) \\ {}_k^s V_R(x) &= \tau_k^i V_L(x) + \rho_k^i V_R(x) \end{aligned} \tag{19}$$

(c) Incident pulse for node (x) at time step $k+1$. Each scattered pulse travels to the boundaries and becomes an incident pulse at the adjacent nodes:

$$\begin{aligned} {}_{k+1}{}^{i}V_L(x) &= {}_k^s V_R(x-1) \\ {}_{k+!}{}^{i}V_R(x) &= {}_k^s V_L(x+1) \end{aligned} \tag{20}$$

The iterative implementation of Eqs. (18) - (20) forms the LL algorithm. It is clear that the main difference between the LR and LL methods is in the calculation of incident and scattered pulses (i.e., Eqs. (11) and (19)). An insulating BC at the right end will be the same as described in Eq. (16). The formulation of the constant-temperature boundary, however, is different for LL and LR models. In an LL model, the transmission line touches the boundary. To keep a constant temperature V_C at the left boundary, a "fictitious" node outside the boundary is assumed together with its corresponding source and transmission line. The temperature at the surface is calculated from the summation of the pulse incident on node 1 at each new time step, and the pulse scattered from node 1 at the previous time step, which should stay constant:

$$_{k+1}{}^{i}V_L(1) = -1{}_k^s V_L(1) + V_C \tag{21}$$

Since the right-hand side of Eq. (21) is known at the present time step, the incident pulse approaching node (x) from the left can be calculated.

2D TLM algorithms follow the general principles discussed in Eqs. (11) to (21) for two perpendicular transmission lines. Following Ref. [12], two TLM codes were developed for LR and LL formulations and implemented in MATLAB for the following case study. A finite difference expression was used in the derivation of m for each node (n) at each time step (k). Following Ref. [15], the mean values of the backward difference forms of the time derivatives were employed to reduce numerical oscillations:

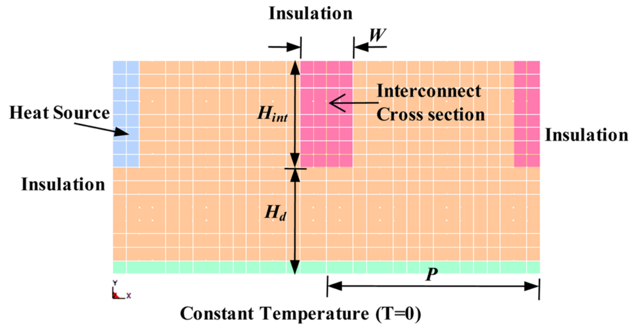

Fig. 3 Schematic of the model consisting of a set of W = 180 nm wide interconnects that are evenly spaced and embedded in the dielectric. The mesh used in the FEA technique is shown. In this study: $H_{int} = H_d = 2W$ and $P = 4W$.

$$_km(n) = \frac{\alpha}{2}\frac{\Delta t^2}{\Delta x^2} \frac{[{}_kV(n) + {}_{k-1}V(n)] - 2[{}_{k-2}V(n) + {}_{k-3}V(n)] + [{}_{k-4}V(n) + {}_{k-5}V(n)]}{[{}_kV(n) + {}_{k-1}V(n)] - [{}_{k-2}V(n) + {}_{k-3}V(n)]} \tag{22}$$

To avoid storing several generations of nodal temperatures at all the nodes, the values of m were calculated at two representative nodes with higher temperatures, one in the interconnect and one in the dielectric.

2D Case Study

A simple case study of interconnect temperature increase for the structure seen in Fig. 3 was performed to evaluate the TLM modeling approach. Simulations of this configuration using FE were used as a basis for the evaluation of the TLM results. This structure closely approximates long, uniformly spaced interconnects [8]. The interconnect aspect ratio is close to 2 for structures found in microprocessors ($H_{int} = 2W$) and the dielectric thickness is approximately equal to the interconnect height ($H_d = 2W$). Interconnect pitch P is variable; we took $P = 4W$ in this study. The bottom surface is fixed at a constant temperature ($T = 0$) and all other surfaces are assumed to be adiabatic. The continuum assumption of our modeling approach was verified by calculating the Knudsen number:

$$Kn = \frac{\lambda}{L} \tag{23}$$

where λ is the molecular mean free path and L the smallest length scale in the problem [13]. The continuum approach is valid as long as $Kn \ll 1.0$. We calculate $Kn = 0.22$ based on the mean free path of copper molecules at 20 °C ($\lambda = 39$ nm) and the width of interconnects ($L = 180$ nm); this justifies that the continuum approach is valid.

The FE model consists of 561 nodes (17×33) and 512 elements. The TLM nodes were selected at the center of FE elements (512 nodes). The interconnect width chosen was $W = 180$ nm, similar to the interconnect width in Ref. [8]. The material properties for the metal and dielectric were specific heat capacity $C_h = 380$ and 1000 J/kgK, density $\rho = 8933$ and 2200 kg/m^3, and thermal conductivity $\kappa = 400$ and 0.17 W/mK, respectively. The comparisons made in this study are for a case when the left-most interconnect is carrying a current density of 10 MA/cm^2 and the volumetric heat generation is 2.2×10^{14} W/m^3 which is calculated using a resistivity of 2.2 $\mu\Omega$-cm.

The FE solver LSDyna (LSTC, Livermore, Calif., USA) for nonlinear multi-physics problems is used, with a variable time step Crank-Nicholson scheme. The FE solver was validated in a

Downloaded From: http://electronicpackaging.asmedigitalcollection.asme.org/ on 01/08/2014 Terms of Use: http://asme.org/terms

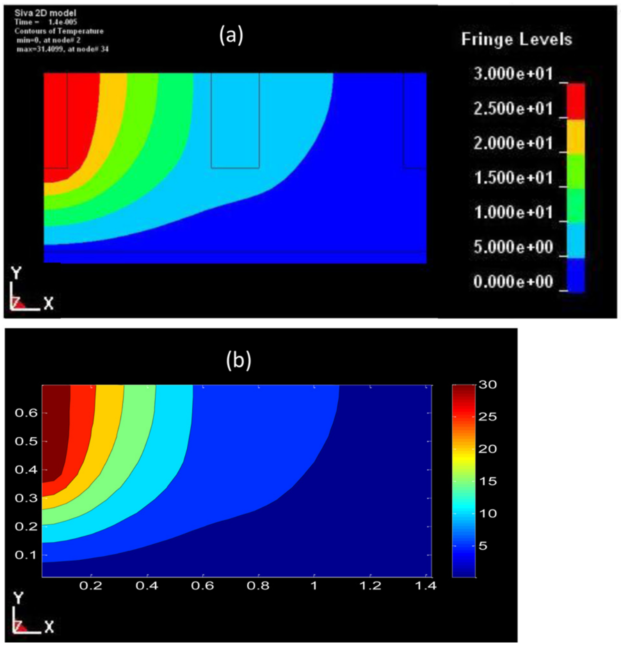

Fig. 4 Temperature contours in the interconnect and dielectric (see Fig. 3) at 14 μs using (*a*) FE method and (*b*) LR TLM method

homogenous 2D problem for which an analytical solution existed [9]. The time step for FE simulations was 1.72 ns.

At each TLM node, considering the inhomogeneity of the model, the resistance and capacitance were defined as [12]

$$R(x,y) = 0.5\frac{dx}{A\kappa(x,y)} \tag{24}$$

$$C(x,y) = Adx\rho(x,y)C_h(x,y) \tag{25}$$

where dx is the length and A is the cross-sectional area of each element, with the thickness equal to 1 μm. The impedance at each node was, therefore,

$$Z(x,y) = \frac{dt}{0.5C(x,y)} \tag{26}$$

The thermal time constant RC of the dielectric material was 25 ns. The TLM time step was chosen smaller than the minimum thermal time constant, i.e., $dt = 10$, 1.0, and 0.1 ns. For comparison, the TLM and FE results were stored at every 1 μs.

The source term in the TLM model was

$$V_{ex}(x,y) = \frac{1}{4}AdxI(x,y)Z(x,y) \tag{27}$$

for the LR model and

$$V_{ex}(x,y) = \frac{1}{4}AdxI(x,y)[Z(x,y) + R(x,y)] \tag{28}$$

for the LL model. In Eqs. (27) and (28), $I(x, y)$ is the volumetric heat source. V_{ex} was added to the nodal temperatures at each iteration.

Results and Comparison

Figures 4(*a*) and 4(*b*) show the results for the spatial variation of temperature at 14 μs from FE and LR TLM respectively. As expected, heat propagates through the structure from left to right and top to bottom due to the heat source at the left-most

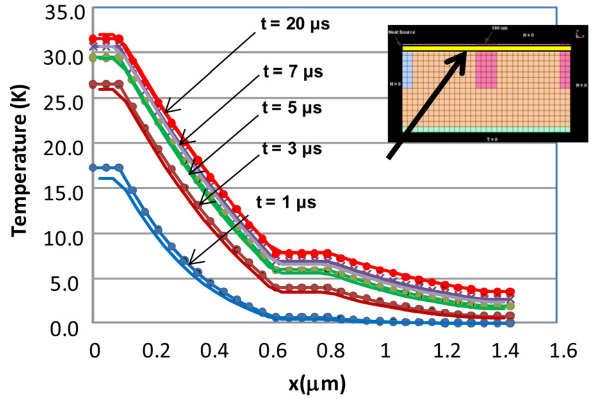

Fig. 5 Comparison of spatial variation of temperature along the x-axis at the upper edge (shown in the picture) by LR TLM (solid line) and FE (marked line) methods at different times

interconnect. The temperature within an interconnect stays almost constant due to its relatively high conductivity. Due to the adiabatic boundary conditions, the temperature contours are perpendicular to the top and left edges.

To get a more detailed comparison of the LR TLM and FE results, the top edge of the structure was selected. Figure 5 demonstrates the comparison of the longitudinal spatial variation of the temperature for the upper edge at five different times between the two models (LR TLM (solid line) and FE (marked line)). The general trend is the decay of temperature along the x-axis. As discussed in Fig. 4, the temperature stays constant along the widths of interconnects. The maximum deviation of the LR TLM from FE results is 7.7%, which happens along the left-most interconnect, where the heat source is located. The difference between the two models decreases along the x-axis from left to right and it also decreases with the increase in time as it gets closer to the steady state.

The analysis of the time step dependency of the LR TLM is demonstrated in Fig. 6. The change of the temperature for the upper edge of the structure along the x-axis is plotted using three values of Δt: 10, 1, and 0.1 ns. It can be seen that, for Δt less than or equal to 1 ns, the results are independent of the Δt. It is important to note that the thermal time constant RC, based on the dielectric properties, was 25 ns. For $\Delta t < 10$ ns, results have a maximum error of 5.8%. The error decreases along the x-axis from left to right.

The transient response of the same structure under identical boundary and initial conditions was studied using the LL TLM as

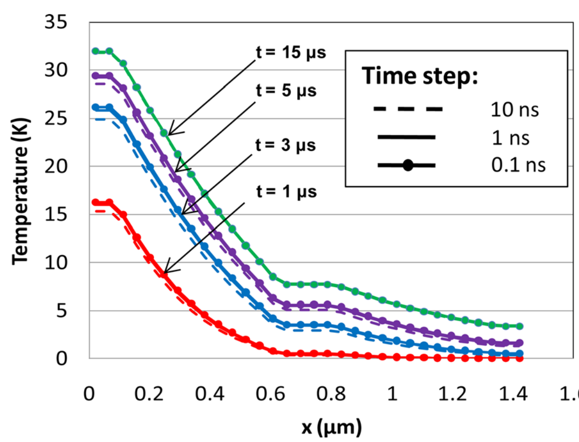

Fig. 6 Analysis of the time step dependency of temperature distribution along the x-axis at the upper edge for LR TLM using time steps of 0.1, 1, and 10 ns

Downloaded From: http://electronicpackaging.asmedigitalcollection.asme.org/ on 01/08/2014 Terms of Use: http://asme.org/terms

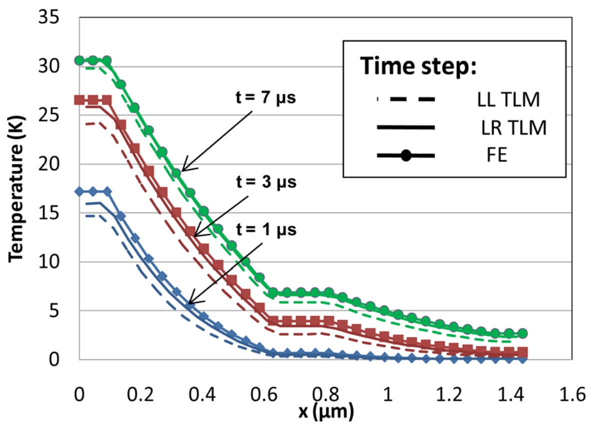

Fig. 7 Comparison of spatial variation of temperature along the x-axis at the upper edge by LR TLM (solid line), LL TLM (dashed line), and FE results (marked line) at three different times

well. Temperature along the x-axis at the upper edge at three different times computed from various methods is shown in Fig. 7. It can be inferred from this figure that LL TLM grows slower than LR TLM. In other words, the transient response of LL TLM lags FE results more than LR TLM and thus, is less accurate. This has also been addressed in Ref. [12]. The difference between the two models, however, decreases along the x-axis as distance from the heat source increases. It also decreases with time.

One of the other differences between the LL and LR TLM is in their dependency on Δt. As discussed earlier for LR TLM, for any Δt smaller than about one tenth of the smallest dielectric *RC*, the model is independent of Δt. In this study for time-steps between 10 ns and 1.92 ns, results are valid and accurate for both models, with a maximum error of 2.8% at steady state. For instance, the variation of temperature in x-direction throughout the structure with time step of 1.95 ns and 1.90 ns are demonstrated in Fig. 8(*a*) and 8(*b*), respectively. However, for LL TLM, $\Delta t < 1.92$ ns causes the model to become unstable. As demonstrated in Fig. 8(*b*), the instability grows from the far right corner of the structure (highlighted in Fig. 8(*c*)) and arises closer to the steady-state situation. It can be seen that the instability also happens at an earlier time as the time step decreases. The source term in the TLM models appears to be an important factor in the numerical oscillations and instabilities mentioned above. Applying smoother input functions, increasing the dimensions of the problem, and using the LR versus LL formulations generally reduce such oscillations [11,12].

The value of *m* is calculated at two points: the upper-left corner (the interconnect region) and at 90 nm to the right of the first point (the dielectric region). The values of *m*, root mean square (RMS) over time for $dt = 1$ ns in the LR model, were 0.268 and 3.69×10^{-5}, respectively, which confirmed that the propagation term in the TLM formulation was negligible. The reason behind choosing the points mentioned is the high temperatures at these locations. In implementing the control of Δt using Eq. (22), it is important to avoid situations that lead to near-zero values of dV/dt ($< 10^{-8}$). Therefore, by averaging the values of *m* with respect to time, the effect of oscillations was eliminated. The RMS values of *m*, for three cases of $dt = 0.1$, 1, and 10 ns are tabulated in Table 1.

The "average computational time" was defined as the ratio of the computational time to the simulation time. This ratio was 4.68 s/μs for FE simulations. For the LR TLM code it was 1.20 s/μs for $dt = 10$ ns and 11.87 for $dt = 1$ ns. Considering that the TLM code was running in MATLAB environment, it can be concluded that, with a standalone executable code, the TLM computational time would decrease.

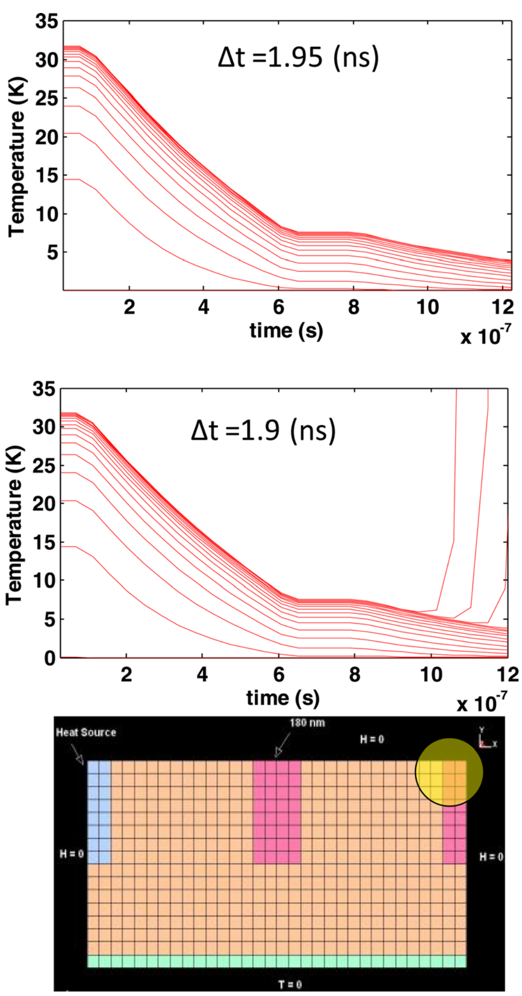

Fig. 8 Observation of the time step dependency of the temperature in LL TLM method along x-axis throughout the structure with time steps of (*a*) $\Delta t = 1.95$ ns and (*b*) $\Delta t = 1.9$ ns. (*c*) Schematic of structure with highlighted region where the instability grows when time step is less than 1.92 ns.

Discussion and Conclusions

In this study, 2D LR and LL TLM algorithms were implemented for transient heat conduction in inhomogeneous arrangements of interconnects and dielectrics. A two-dimensional case study was presented and the TLM results were compared with the transient FE results. The overall behavior of the TLM models was similar to the FE model while, near the heat source, the transient TLM solutions developed slower than the FE solution. The issue of inaccuracy due to a voltage source being added at the boundary has been addressed previously by investigators such as Ref. [12]. The steady-state results of the two models were in good agreement with a maximum error of 2.8%.

Table 1 The RMS values of *m* calculated at two points: the upper-left corner (the interconnect region) and at 90 nm to the right of the first point (the dielectric region) for three cases of *dt* = 0.1, 1, and 10 ns

	RMS value of "*m*"	
time step (ns)	interconnect with the source	dielectric adjacent to the source
10 ns	15.730	0.006
1 ns	0.268	3.69×10^{-5}
0.1 ns	0.0003	1.96×10^{-7}

Downloaded From: http://electronicpackaging.asmedigitalcollection.asme.org/ on 01/08/2014 Terms of Use: http://asme.org/terms

Two distinct TLM formulations, LR and LL, were implemented and compared. The two formulations yielded slightly different transient results, with the LL result growing slower, particularly at the source boundary. The LR formulation results were closer to the FE results. It was shown that the stability of the LL results depends on the time step. Below a maximum time step, the LL results showed instability that started from the insulating boundary. Similar observations have been reported by Refs. [11] and [12], who indicated that the LR formulation is more accurate for transient thermal analysis.

An important feature to be added to this study is the use of a special type of mesh refinement called quad-tree mesh. Quad-tree mesh has the ability to increase the mesh resolution dramatically in a rather short length scale and; therefore, to generate a non-uniform mesh along different directions. Using a quad-tree mesh with TLM method, an inhomogeneous multi-scale structure can be simulated in a reasonable simulation time by having locally refined mesh resolution at points of interests.

In the transient solution of heat diffusion equation, the initial time step should be smaller than the thermal time constant for the physics of the problem to be captured accurately. However, for a constant heat source, as the solution reaches the steady state, the rate of change of temperature as a function of time decreases. An important feature of the TLM model is the ability to accept a variable time step. Therefore, by using an adjustable time step during the TLM simulation, the computational time can be dramatically decreased [9].

Acknowledgment

The funding for this study was provided by Semiconductor Research Corporation (SRC) under task 1883.001.

References

[1] Phan, T., Dilhaire, S., Quintard, V., Lewis, D., and Claeys, W., 1997, “Thermomechanical Study of AlCu Based Interconnect Under Pulsed Thermoelectric Excitation,” J. Appl. Phys., **81**, pp. 1157–1157.
[2] Evans, J. W., Evans, J. Y., Lall, P.,and Cornford, S. L., 1998, “Thermomechanical Failures in Microelectronic Interconnects,” Microelectron. Reliab., **38**, pp. 523–529.
[3] Bastawros, A. F., and Kim, K. S., 1998, “Experimental Study on Electric-Current Induced Damage Evolution at the Crack Tip in Thin Film Conductors,” Trans. ASME J. Electron. Packag., **120**, pp. 354–359.
[4] Bilotti, A. A., 1974, “Static Temperature Distribution in IC Chips with Isothermal Heat Sources,” IEEE Trans. Electron Devices, **ED-21**, pp. 217–226.
[5] Teng, C. C., Cheng, Y.-K., Rosenbaum, E., and Kang, S.-M., 2002, “iTEM: A Temperature-Dependent Electromigration Reliability Diagnosis Tool,” IEEE Trans. Comput.-Aided Des., **16**, pp. 882–893.
[6] Chen, D. Li, E., Rosenbaum, E., and Kang, S.-M., 2002, “Interconnect Thermal Modeling for Accurate Simulation of Circuit Timing and Reliability,” IEEE Trans. Comput.-Aided Des., **19**, pp. 197–205.
[7] Stan, M. R., Skadron, K., Barcella, M., Huang, W., Sankaranarayana, K., and Velusamy, S., 2003, “HotSpot: A Dynamic Compact Thermal Model at the Processor-Architecture Level,” Microelectron. J., **34**, pp. 1153–1165.
[8] Gurrum, S. P., Joshi, Y. K., King, W. P., Ramakrishna, K., and Gall, M., 2008, “A Compact Approach to On-Chip Interconnect Heat Conduction Modeling using the Finite Element Method,” J. Electron. Packag., **130**, p. 031001.
[9] Smy, T., Walkey, D., and Dew, S. K., 2001, “Transient 3D Heat Flow Analysis for Integrated Circuit Devices using the Transmission Line Matrix Method on a Quad Tree Mesh,” Solid-State Electron., **45**, pp. 1137–1148.
[10] Christopoulos, C., 1995, *The Transmission-Line Modeling Method TLM*, IEEE Press, New York.
[11] De Cogan, D., O’Connor, W. J., and Pulko, S., 2006, *Transmission Line Matrix in Computational Mechanics*, CRC, Boca Raton, FL.
[12] Ait-sadi, R., and Naylor, P., 1993, “An Investigation of the Different TLM Configurations used in the Modelling of Diffusion Problems,” Int. J. Numer. Model., **6**, pp. 253–268.
[13] Zhang, Z. M., 2007, *Nano/Microscale Heat Transfer*, McGraw-Hill Professional, New York.
[14] Johns, P. B., 1977, “A Simple Explicit and Unconditionally Stable Numerical Routine for the Solution of the Diffusion Equation,” Int. J. Numer. Methods Eng., **11**, pp. 1307–1328.
[15] Gui, X., Webb, P. W., and De Cogan, D., 1992, “An Error Parameter in TLM Diffusion Modelling,” Int. J. Numer. Model., **5**, pp. 129–137.

Downloaded From: http://electronicpackaging.asmedigitalcollection.asme.org/ on 01/08/2014 Terms of Use: http://asme.org/terms